Calculating and communicating ensemble-based volcanic ash dosage and concentration risk for aviation

Calculating and communicating ensemble-based volcanic ash dosage and concentration risk for aviation

Andrew T. Prata,[a]* Helen F. Dacre,[a] Emma A. Irvine,[a] Eric Mathieu,[a] Keith P. Shine[a] and Rory J. Clarkson[b]

[a]*Department of Meteorology, University of Reading, UK*

[b]*Engine Environmental Protection, Rolls-Royce plc, Derby, UK*

ABSTRACT: During volcanic eruptions, aviation stakeholders require an assessment of the volcanic ash hazard. Operators and regulators are required to make fast decisions based on deterministic forecasts, which are subject to various sources of uncertainty. For a robust decision to be made, a measure of the uncertainty of the hazard should be considered but this can lead to added complexity preventing fast decision making. Here a proof-of-concept risk matrix approach is presented that combines uncertainty estimation and volcanic ash hazard forecasting into a simple warning system for aviation. To demonstrate the methodology, an ensemble of 600 dispersion model simulations is used to characterise uncertainty (due to eruption source parameters, meteorology and internal model parameters) in ash dosages and concentrations for a hypothetical Icelandic eruption. To simulate aircraft encounters with volcanic ash, trans-Atlantic air routes between New York (JFK) and London (LHR) are generated using time-optimal routing software. This approach has been developed in collaboration with operators, regulators and engine manufacturers; it demonstrates how an assessment of ash dosage and concentration risk can be used to make fast and robust flight-planning decisions even when the model uncertainty spans several orders of magnitude. The results highlight the benefit of using an ensemble over a deterministic forecast and a new method for visualising dosage risk along flight paths. The risk matrix approach is applicable to other aviation hazards such as SO_2 dosages, desert dust, aircraft icing and clear-air turbulence and is expected to aid flight-planning decisions by improving the communication of ensemble-based forecasts to aviation.

KEY WORDS ash concentration; ash dosage; dispersion modelling; risk matrix; aviation; flight planning; ensemble forecasting

1. Introduction

Flight-planning decisions during volcanic eruptions pose many challenges to the aviation industry. An important issue in the decision-making process is the economic impact of grounding and re-routing aircraft during an eruption event and the potential for damage to the engines due to flying in ash clouds at low concentration levels that do not cause an immediate safety risk. While aircraft encounters with volcanic ash are a known safety issue (Casadevall, 1994; Prata and Tupper, 2009; Guffanti and Tupper, 2015), there have been many incidents which suggest that aircraft engines can tolerate low concentrations of ash without catastrophic engine failure. A total of 131 incidents were reported between 1953–2009 and a further 122 were documented for the period from 2010–2016 (Guffanti *et al.*, 2010; Christmann *et al.*, 2017). The increase in documented aircraft encounters between 2010–2016 may be partly a result of better reporting and the publicity of the 2010 Eyjafjallajökull eruption in Iceland. However, as the number of aircraft flying in volcanically active regions around the globe continues to grow—Airbus projects a doubling of passenger aircraft from 2017–2036 (Airbus, 2017)—the number of aircraft encounters with volcanic ash and gas clouds are likely to increase with the potential to lead to serious global economic impacts. In this paper a new way of calculating and communicating volcanic ash forecasts which allows the aviation community to assess the risks associated with flying along a given route and to make flight-planning decisions is presented.

The eruptions of Eyjafjallajökull (Iceland) in April and May 2010 had a profound economic impact on the aviation industry. So much so that it prompted changes to the approach taken by regulators towards flying in ash-contaminated airspace. At the time, the International Civil Aviation Organization (ICAO) recommended that all encounters with volcanic ash clouds should be avoided, regardless of the ash concentration (ICAO, 2007). This approach became unworkable during the crisis which put pressure on regulators to re-open controlled airspace where ash concentrations were forecast to be low. In response, the UK Civil Aviation Authority (CAA) in consultation with Rolls-Royce, the UK Met Office, international and European regulators and aviation experts developed quantitative peak concentration limits (Witham *et al.*, 2012; Clarkson *et al.*, 2016). Currently, the ICAO EUR/NAT (European and North Atlantic) Volcanic Ash Contingency Plan uses peak concentration limits to define low ($\leq$ 2 mg m^{-3}), medium (2–4 mg m^{-3}) and high ($\geq$ 4 mg m^{-3}) ash contamination levels (ICAO, 2016). The European Aviation Safety Agency (EASA) and UK CAA have adopted these ash contamination levels and operators are required to have a Safety Risk Assessment approved by their National Aviation Authority before considering entering airspace forecast to contain medium or high ash contamination levels (CAA, 2017).

The UK Met Office and Météo-France currently provide quantitative peak concentration forecasts (defined in Section 2) as supplementary information to Volcanic Ash Advisories and Volcanic Ash Graphics issued by the London and Toulouse Volcanic Ash Advisory Centres (VAACs), respectively. Peak concentrations, however, do not take into consideration the situations where an aircraft may be flying through a low concentration ash cloud for a long period of time, which may lead to engine damage (Wylie *et al.*, 2017), or a moderate concentration for a relatively short period of time, which may not lead to engine damage. Volcanic ash dosages represent the accumulated concentration over time along an aircraft's route, thus accounting for the situations above.

Recently, Rolls-Royce announced an ash dosage threshold below which exposures will not lead to significant reductions in flight safety margins (Rolls-Royce, 2017). Up to ash concentrations of 4 mg m^{-3} the threshold has been set at a dosage of 14.4 g m^{-3} s. This value was calculated based on the assessment that a Rolls-Royce engine should be able to maintain all safety margins after spending 1 h in a concentration of 4 mg m^{-3} or 2 h in a concentration of 2 mg m^{-3}. As a result of limitations set by EASA the appropriate dosage above 4 mg m^{-3} has not been defined. These recent developments motivate the need to develop a framework that combines quantitative ash concentration forecasts with air route data to quantify ash dosages along flight paths and their uncertainties.

The move to quantitative ash concentration limits has driven rapid development and improvement in volcanic ash concentration forecasting (e.g. Stohl *et al.*, 2011; Dacre *et al.*, 2011; Devenish *et al.*, 2012; Millington *et al.*, 2012; Webster *et al.*, 2012). However, dispersion model simulations are subject to various sources of uncertainty which are currently not taken account of by operational deterministic forecasts. Communicating this uncertainty to aviation stakeholders is of prime importance as this information can be used to make better-informed decisions (Mulder *et al.*, 2017).

The major sources of uncertainty in volcanic ash transport and dispersion models include uncertainty in the eruption source parameters (e.g. mass eruption rate and plume height), internal model parameterisations (e.g. wet deposition and free tropospheric turbulent mixing) and the driving meteorology (Folch, 2012; Harvey *et al.*, 2018). The challenge is then to develop a robust methodology which accounts for these uncertainties objectively, but also allows for fast decisions to be made by operators and regulators. Robust decisions from quantitative data require a measure of their uncertainties. A common method for representing uncertainty in weather forecasting is to develop an ensemble: a set of model realisations created by perturbing various uncertain parameters used at the start of each model run (e.g. Palmer, 2002; Buizza *et al.*, 2005; Gneiting and Raftery, 2005). An ensemble (probabilistic) forecast allows for a robust decision as it can be used to quantify the likelihood of a certain event occurring. It is therefore logical to extend ensemble forecasting methods to dispersion modelling of volcanic ash concentrations. An example in the context of the ash–aviation problem would be the likelihood of the ash concentration being above a certain threshold. However, too much (or too complex) information can prevent a decision-maker from making a fast decision, which is generally a requirement in operational settings. This issue is often referred to as 'information overload' and was raised as a major concern by operators and regulators during and following the 2010 Eyjafjallajökull crisis.

The UK Met Office National Severe Weather Warning Service utilises the concept of a risk matrix to communicate ensemble-based forecasts of severe weather events to the public (Neal *et al.*, 2014). *Risk* is defined as the product of the *likelihood* and *impact* of an event occurring. A risk matrix is constructed by discretising likelihoods and impacts into different ranges and assigning a risk severity to each combination of the impact and likelihood ranges. This approach addresses the issue of information overload by condensing probabilistic information into appropriate courses of action to be taken by the relevant stakeholders (e.g. the public, an airline operator, emergency services etc.). In the present study, this approach is adapted to the ash–aviation problem by considering ash dosage and peak concentration as *impact* and using ensemble modelling to quantify their *likelihood*.

The aim of this paper is to develop a proof-of-concept methodology for implementing a risk-based approach to flight planning; using ash dosage and concentration encountered by an aircraft along its flight path (hereafter known as 'along-route ash dosage and/or concentration'). To generate ash concentration data, a hypothetical Icelandic eruption scenario resulting in ash dispersal across the North Atlantic was simulated using the dispersion model used operationally by the London VAAC (LVAAC). Trans-Atlantic air routes were generated using time-optimal routing software to simulate ash encounters permitting ash dosage calculations. An ensemble dataset was developed (based on uncertainty in the meteorology, eruption source parameters and internal model parameterisations) to estimate the likelihood of certain ash dosage and peak concentration ranges. The ash dosage risk was then calculated for various flight routes to demonstrate how airline operators might use this information.

2. NAME model setup

The Numerical Atmospheric-dispersion Modelling Environment (NAME; Jones *et al.*, 2007) is a Lagrangian dispersion model used operationally by the LVAAC. The Lagrangian representation of atmospheric dispersion within NAME allows for each model particle to be tracked as it is advected by the three-dimensional wind fields. If the size (volume), shape and density of a particle are known its mass can be calculated. Mass concentration fields are calculated in NAME by dividing the total mass of particles in a given grid box by its volume.

In the present study, NAME (version 6.5) was used to simulate a hypothetical Icelandic eruption using the default setup of the LVAAC. Ash (mass) concentrations were output onto a global grid of 800 by 600, corresponding to a grid resolution of approximately 0.451 ° longitude by 0.301 ° latitude (~40 km horizontal resolution), at 22 flight levels (FL) from FL000 to FL550 (1013.25 to 91.15 hPa) with a vertical resolution of 25FL. Note that flight levels are defined as standardised pressure altitudes expressed in units of hundreds of feet and are based on the ICAO standard atmosphere. The concentration fields were output every 6 h using a 6 h time average with a total run time of 66 h. The eruption plume was defined as a uniformly distributed vertical line source extending from the volcano summit to the eruption plume height and the particle release rate was set to 15000 h^{-1}, which is consistent with the model set up at the LVAAC (Witham *et al.*, 2016). Finally, to convert to peak concentrations, the mean ash concentration fields output by NAME were multiplied by a factor of 10. This is known as the 'peak-to-mean' factor and has been adopted by the LVAAC to account for peak concentrations that cannot be resolved by the NAME model (Webster *et al.*, 2012). This model configuration is referred to as the 'thin layer' setup hereafter and is equivalent to the '25FL layer scheme' described in Webster *et al.* (2012). The output from the thin layer setup in NAME was then post-processed to produce the LVAAC's 'thick layer' product. The 'thick layer' product was produced by dividing the vertical grid into three flight level ranges (FL000–FL200, FL200–FL350 and FL350–FL550) and then setting the maximum ash concentration of the thin layers (25FL thickness) within each range to the concentration of each thick layer (Figure 1).

2.1. Meteorological data

The meteorological data that were used to drive NAME includes two datasets: an analysis dataset produced by the Met Office Unified Model (MetUM; Cullen, 1993; Brown *et al.*, 2012) and an ensemble dataset produced using the European Centre for Medium-Range Weather Forecasts (ECMWF) Integrated Forecast System (IFS) (Buizza *et al.*, 1999). The MetUM analysis fields have a horizontal resolution of ~17 km and vertical resolution of ~0.7 km in the upper troposphere/lower stratosphere (UTLS). The time resolution of the MetUM data is 3 hourly alternating from analysis to forecast fields every 3 h. At time intervals smaller than 3 h, the meteorology fields are linearly interpolated. The MetUM dataset was used to drive NAME for the control run (described in Section 2.2). The ECMWF IFS (cycle 43r1) was used to create an ensemble of forecast meteorology. These data were archived at a horizontal resolution of 16 km (T1279 spectral truncation) and vertical resolution of ~1.4 km in the UTLS with a time resolution of 3 h and forecast lead-time of 66 h. These data were then extracted onto a regular latitude/longitude grid of 0.125 º by 0.125 º and the precipitation, surface stresses and sensible heat flux fields were post-processed so that they could be read in by NAME. To account for uncertainty in the initial meteorological fields, the ECMWF IFS Ensemble Prediction System (EPS) was used to produce a 20-member meteorological ensemble. The EPS utilises the singular-vector approach (Buizza and Palmer, 1995) to perturb initial conditions in the meteorology and a stochastic physics scheme (Buizza *et al.*, 1999) to account for model uncertainty. The ECMWF dataset was used to investigate four sources of uncertainty in dispersion modelling: eruption source parameters, internal NAME model parameters, initial meteorological conditions and error growth with increasing forecast lead-time.

2.2. Icelandic eruption scenario

The parameters used to define an eruption in NAME are referred to as eruption source parameters (ESPs). These include the timing, location, duration, plume height, geometry and vertical ash distribution of each eruptive phase during an event as well as the mass eruption rate (MER) and microphysical properties of the distal fine ash particles (shape, density and size distribution). In the following, the control run ESPs for the Icelandic eruption scenario are described.

An explosive eruption from an Icelandic volcano has the potential to release volcanic ash at aircraft cruising altitudes. Depending on the weather conditions, this type of eruption could result in widespread ash dispersal across the North Atlantic and neighbouring landmasses, disrupting trans-Atlantic air-traffic. The Katla volcano (19.083 ° W, 63.633 ° N, 1490 m a.s.l.) was selected for the eruption scenario as it is an active volcano in Iceland with the potential for an explosive ash-rich eruption. The eruption plume height was set to 15 km a.s.l. with a duration of 16 h to ensure significant ash dispersal at cruise altitude (~10 km). Following the current approach of the LVAAC, the MER was calculated from the plume height using the empirically-derived Mastin *et* *al.* (2009) relationship. As the total grain size distribution is not modelled in NAME, the fraction of mass due to fine ash (diameters ≤ 100 μm) must be considered. This is known as the distal fine ash fraction (DFAF) and is also included as an ESP here. As the DFAF is the percentage of mass assumed to remain in the atmosphere after an initial eruption, the MER is scaled by this percentage. A DFAF of 5% was chosen as this is the default value used by the LVAAC for an Icelandic eruption (Witham *et al.*, 2016). Similarly, the LVAAC's default ash size distribution was used (see Witham *et al.*, 2016 Table 1) and the shape of the particles were assumed to be spherical.

The eruption start time was set to 1 January 2017 at 0300 UTC as during this time an upper-level ridge had formed over Iceland and the North Atlantic Ocean. This winter-time weather regime is representative of the W3 and W4 categories identified by Irvine *et al.* (2013) as frequent modes of variability in the North Atlantic. This meteorological situation occurs one third of the time during the winter months and is characterised by northerly flow from Iceland and persistent anticyclonic flow over the North Atlantic. In this scenario, volcanic ash from an Icelandic eruption is dispersed toward the south and circulated over the North Atlantic for several days. Due to large scale subsidence there is very little precipitation in this scenario and so the amount of wet deposition is expected to be small. The control run ESPs are summarised in Table 1 and the evolution of the ash cloud over 66 h in the control run simulation for the thick layer concentrations from FL350–FL550 is shown in Figure 2.

3. Ensemble simulations

There are many ways to represent uncertainty in model simulations. In this paper, an ensemble of NAME simulations is created by varying the meteorology, ESPs and internal model parameters. Latin Hypercube Sampling (LHS; Iman and Conover, 1980) is a statistical technique that can be used to efficiently generate an ensemble which ensures orthogonality between input model parameter sets. The LHS method was used to generate a Latin Hypercube with 9 dimensions (i.e. 9 dispersion model input parameters were varied) and was sampled 600 times resulting in an ensemble of 600 members. These simulations were conducted on the JASMIN 'super-data-cluster' (Lawrence *et al.*, 2012) and took less than 1 h to complete for a 24-h ensemble forecast. This runtime (and ensemble size) potentially allows an operational VAAC to provide 24 h ensemble forecasts every 6 h; provided that they have sufficient computer resources and an operational meteorological ensemble prediction system set up. All model parameters considered in the LHS analysis were sampled from a uniform distribution. By sampling from a uniform distribution, it is assumed that all values between their specified ranges are equally likely. The 9 model parameter choices (and their specified ranges) are listed in Table 1 and are described in the following sections.

3.1. Meteorological initial conditions and forecast error growth

It has been demonstrated that even for short lead-time forecasts (< 72 h) small differences in the forecast wind fields can lead to large spread in the forecast ash clouds (Dacre and Harvey, 2018). As described in Section 2.1, uncertainty in the initial meteorological fields as well as error growth in the forecast fields were represented using the ECWMF dataset. These data make up a 20-member ensemble of meteorology. For the LHS sampling, ECMWF members were sampled from a uniform distribution between 0 and 19. The random variable sampled from this range was then rounded to the nearest integer. This index was then used to select (at random) an ECMWF ensemble member for each of the 600 parameter sets.

3.2. Eruption source parameters

To represent the uncertainty associated with the ESPs, a range of uncertainty (i.e. maximum and minimum values) was assigned to each control run ESP and then randomly sampled from a uniform distribution between the specified ranges (Table 1). The plume height, DFAF and MER were selected for the LHS analysis as output from NAME has been shown to be the most sensitive to these parameters (e.g. Dacre *et al.*, 2011; 2013; Harvey *et al.*, 2018). The source timing (i.e. eruption onset) and duration were chosen to illustrate how uncertainty in these parameters can lead to uncertainty in the timing and location of the modelled ash cloud.

The ranges selected for each ESP were made based on typical ranges reported in the literature (e.g. Mastin *et al.*, 2009; Devenish *et al.*, 2012; Dacre *et al.*, 2013; Harvey *et al.*, 2018). It is acknowledged that there is a degree of subjectivity in these choices; however, their specific values do not alter the methodology developed to implement a risk-based approach (described in Section 6) that can be used for making robust and fast flight-planning decisions.

3.3. Internal model parameters

Dacre *et al.* (2015) have shown that the internal model parameters used in NAME to represent free tropospheric turbulence can significantly impact the vertical depth (thickness) of volcanic ash clouds and hence peak concentrations. These internal model parameters were also investigated by Harvey *et al.* (2018) and were demonstrated to be the largest internal model parameter contribution to uncertainty in NAME output. To represent uncertainty in free tropospheric turbulence, the standard deviation (σ) and Lagrangian timescales (τ) of the horizontal and vertical velocity components were sampled from a uniform distribution using the range specified in Harvey *et al.* (2018). The horizontal and vertical components of these parameters were varied in proportion to each other so that the shape of the turbulent eddies parameterised in NAME is preserved. It is also noted that the horizontal component of standard deviation of the free tropospheric turbulence was sampled on a logarithmic scale. Finally, the standard deviation of the horizontal velocity for unresolved mesoscale motions was also sampled from a uniform distribution following the ranges used in Harvey *et al.* (2018).

4. Along-flight ash dosage

To simulate aircraft encounters with volcanic ash, flight routes were generated using time-optimal routing software developed by Irvine *et al.* (2016), which was based on the methodology of Lunnon and Marklow (1992). The 'flightCode' program uses latitude and longitude pairs representing the origin and destination airports for a given route, the constant true airspeed of the aircraft and horizontal wind data at a given flight level. The code assumes that the aircraft is at a fixed altitude and so take-off and landing are not considered. The output of flightCode is a set of waypoints (latitude and longitude pairs) representing the fastest (time-optimal) route for the specified airport pairs at a given instance in time given the prevailing wind at a given altitude.

In the present analysis, trans-Atlantic flights were generated assuming a constant true airspeed of 250 m s^{-1} (900 km h^{-1}) and the MetUM dataset was used to provide horizontal wind data at FL350 (assumed to be the cruise altitude of the aircraft). The eastbound and westbound time-optimal routes from New York (JFK) to London (LHR) were calculated for each time step of the dispersion model output (i.e. at 6 h intervals for 11 time steps).

The along-flight ash dosage is defined as the ash concentration multiplied by the time spent in that concentration (duration of exposure) along an aircraft's flight path, which means that the dosage, D, is expressed in units of grams per cubic metre seconds (g m^{-3} s):

$$D = \sum_{i=1}^{n} C_i \Delta t_i = \sum_{i=1}^{n} C_i \frac{\Delta s_i}{V_a} \quad (1)$$

where n is the number of dispersion model grid boxes intersected by the air route, Δt_i is the duration of exposure in the ith grid box, C_i is the ash concentration of the ith grid box intersected, Δs_i is the distance travelled through the ith grid box and V_a is the true airspeed of the aircraft. This definition means that dosage always increases monotonically along the route and is distinct from Peterson and Dean (2007) who use 'ash exposure' (g m^{-2}) to quantify the potential damage to aircraft intersecting ash clouds and Prata and Prata (2012) who defined dosage as the accumulated mass of ash (g) along an aircraft's route. The definition adopted here (g m^{-3} s) is consistent with the definitions used in Kristiansen *et al.* (2015), Clarkson *et al.* (2016), Wylie *et al.* (2017) and Prata *et al.* (2018); however, Clarkson *et al.* (2016) refer to dosage as a 'dose' in their paper. All dosage calculations reported here assume that the modelled ash concentration fields at a given time step are static (i.e. do not change with time) as the aircraft flies from the origin to destination at its true airspeed. Note also that these ash concentrations correspond to the post-processed ash concentrations at the FL350–FL550 thick layer level (described in Section 2) and may result in overestimates of the along-route dosage at FL350 due to the application of the peak-to-mean ratio and the approach of taking the maximum concentration of the thin layers between FL350 and FL550 when determining the 'thick layer' concentration.

5. Representation of uncertainty

5.1. Model agreement maps

The ensemble simulations (described in Section 3) were used to calculate the likelihoods of ash concentrations exceeding different thresholds, based on output from NAME. Specifically, the likelihoods represent the percentage of ensemble members that predicted an ash concentration above a certain peak concentration threshold. Based on discussions with regulators and operators these likelihoods were split into three ranges: less likely (0–10%), likely (10–90%) and very likely (90–100%). It is noted that while regulators and operators suggested a three-category system, the actual values of these boundaries were chosen by the authors to illustrate the present method. In an operational setting, these values may be altered by the user to reflect their risk appetite. Given that these percentages represent the level of agreement between ensemble members these maps are referred to hereafter as ‘model agreement maps’ and do not strictly constitute likelihoods. For ensemble simulations to represent true likelihoods they should be calibrated using past observations and forecasts. However, in order to illustrate the proof-of-concept risk matrix method in this paper, uncalibrated ‘model agreement’ values are used to represent ‘likelihoods’ (described in Section 6). The likelihood boundaries represented on the model agreement maps, however, depend on the ash concentration threshold chosen. The choice of threshold was raised in meetings with various aviation stakeholders and thresholds ranging from 0.2–10 mg m^{-3} were suggested.

To demonstrate how model agreement maps depend on ash concentration thresholds, four model agreement maps (for FL350–FL550 at T+30) were generated; corresponding to four ash concentration thresholds: 0.2, 2, 4 and 10 mg m^{-3}. Figures 3(a)–(d) show both the horizontal and vertical model agreement maps for each of the peak concentration thresholds analysed. Note that the vertical cross-sections were constructed by first calculating the time-optimal route at FL350 from JFK to LHR (return) and then calculating the ash concentration along this route for each thick layer level. The ash concentration contours corresponding to each peak concentration threshold from the control run are also overlaid on Figures 3(a)–(d) to demonstrate where an ash cloud boundary might be drawn for a single (deterministic) forecast.

The horizontal model agreement maps reveal regions where there is high confidence in the location of the ash cloud and concentration and regions where there is low model confidence. Figure 3(a) shows the 0.2 mg m^{-3} ash concentration contour for the control run, which may be used to determine the extent of a modelled ash cloud (Witham *et al.*, 2012). The model agreement map indicates that over the western part of the British Isles a considerable percentage (>10%) of ensemble member simulations contained ash above 0.2 mg m^{-3} whereas the control simulation (black line) did not. This result demonstrates that, for this scenario, a single (deterministic) model simulation would not have forecast ash concentrations above 0.2 mg m^{-3} over this region while the ensemble, which accounts for uncertainty in the deterministic simulation, shows that ash over this region was 'likely' (10–90%). Comparison of the different ash concentration thresholds demonstrates that when the threshold is increased the region of uncertainty increases relative to the control run (deterministic forecast). This is illustrated by Figure 3(d) where the control run contour of 10 mg m^{-3} covers a small region over the middle section of the westbound flight path and the ensemble indicates that ash concentrations above 10 mg m^{-3} are 'likely' (10–90%) over a larger region of the North Atlantic. The region of uncertainty relative to the control run also increases with increasing ash concentration threshold for the vertical model agreement maps, where this approach quantitatively shows the degree of confidence in the model for ash concentrations at the three thick layer regions. In the bottom panel of Figure 3(a), at approximately 5000 km along the route, the control run simulation indicates ash at low altitudes; however, the model agreement contours indicate that > 10% of the ensemble members resulted in ash concentrations above 0.2 mg m^{-3} at cruise altitude (FL350–FL550 thick layer level).

In general, the area covered by each likelihood category was reduced as the ash concentration threshold was increased (compare Figures 3(a)–(d)); however, the uncertain region over the western part of the British Isles remained largely the same for thresholds up to 10 mg m^{-3} (Figures 3(a)–(d)). This indicates that 10–90% of the ensemble members forecast ash concentrations above 10 mg m^{-3} over this region (Figure 3(d)).

5.2. Model agreement along routes

The ensemble approach can also be used to represent the uncertainty in ash dosage calculations. However, as the dosage is calculated along a flight path, the model agreement values are displayed as the percentage of ensemble members that predict the dosage to be above a certain dosage threshold along the air route. Figure 4(a) shows the model agreement along the route from JFK–LHR (return) at FL350–FL550 and T+30 using the Rolls-Royce airworthiness threshold of 14.4 g m^{-3} s. When the model agreement is calculated along the route, the likelihood of the aircraft engine exceeding the dosage threshold increases along the route. For comparison, Figure 4(b) shows the same model agreement along the route but for a doubling of the dosage threshold (i.e. 28.8 g m^{-3} s). As with the ash concentration model agreement maps, when the dosage threshold is increased, the likelihood categories are affected. For this example, when the dosage threshold is doubled, the distance the aircraft can travel while remaining in the 'likely' category increased by a small amount while the distance travelled in the 'very likely' category reduced (compare Figures 4(a) and (b) at the location of the westbound aircraft). This small difference suggests that an operator may make a similar decision for both dosage thresholds for this particular scenario. However, for a different air-route or eruption scenario a change in the dosage threshold may have more of an effect on the likelihood boundaries.

Displaying model agreement as maps and along air routes provides aviation stakeholders with a new method for displaying ensemble-based ash concentration and dosage information. While this approach has been demonstrated for the JFK–LHR route, operators could apply the same analysis to different or multiple flight tracks. The main advantage in displaying the data this way is that decision-makers are provided with information about the confidence of the model forecasts, which may improve flight-planning procedures.

6. Risk maps and routes

While the concept of model agreement is useful in that it can be used to indicate the likelihood of a given impact (e.g. ash concentration and dosage) at a certain flight level and time, multiple figures must be generated for varying thresholds of interest and may prevent an operator from making a fast decision due to information overload. A risk-based approach has been shown to reduce this issue for other hazards by condensing the ensemble information into a single map (e.g. Neal *et al.*, 2014); thereby permitting multi-layered information in operational settings and providing the users with the relevant information needed to make a decision.

6.1. Ash concentration risk matrix

To construct a risk matrix both the impact and likelihood of the hazard must be combined (shown schematically in Figure 5(a)). For the ash concentration risk matrix, the impact was defined based on the following ash concentration (C) ranges (in mg m^{-3}): $0.2 < C \leq 2$, $2 < C < 4$ and $C \geq 4$. For the likelihood ranges, the same ranges in Section 5 were used: 0–10 % (less likely), 10–90 % (likely) and 90–100 % (very likely); resulting in a 3 by 3 matrix (Figure 5(b)).

The boxes in the risk matrix each correspond to a different combination of impact and likelihood. Following the approach of Neal *et al.* (2014), each box was assigned a colour using a three-colour warning system (yellow, amber and red). The colours then correspond to a decision to be made or action to be taken by the stakeholder. For example, if it is very likely (90–100%) that the peak concentration will be low (0.2–2 mg m^{-3}) the risk level is shown in the top left box of the ash concentration risk matrix (Figure 5(b)). The decision of a flight-planner in this situation might be to allow the aircraft to fly its scheduled route and continue to check updated forecasts. On the other hand, if it is very likely (90–100%) that the peak concentration will be high ($\geq$ 4 mg m^{-3}) the risk level is shown in the top right box of the matrix. In this situation a different action might be taken such as re-routing the aircraft. To illustrate how the risk matrix might be used to make fast and robust decisions, the following example actions were assigned to each colour warning (Figure 5(c)):

1) Yellow = Schedule route; check updated forecasts
2) Amber = Load more fuel; check updated forecasts; perform engine checks
3) Red = Consider alternative routes

Figures 6(a) and (b) show risk maps in the horizontal and vertical, respectively, for the same valid meteorological time and altitude shown in Figure 3. Note that at each location on the risk maps the colour warning corresponding to the maximum risk level is shown. For example, in a location where the likelihood of the ash concentration exceeding 4 mg m^{-3} is less likely (i.e. an amber warning) and the likelihood of the ash concentration being 0.2–2 mg m^{-3} is likely (yellow warning), the latter is ignored in favour of the higher risk level. The horizontal risk map (Figure 6(a)) shows that amber and red warnings would be issued for airspace over the western part of the British Isles while the areas between Iceland and the British Isles and over large parts of the

North Atlantic would be issued with red (high risk) warnings. In this situation, the decision for aircraft planning routes over the amber regions of the risk map could be to load more fuel and perform engine checks. Figure 6(b) shows that aircraft flying the time-optimal eastbound and westbound routes between JFK and LHR at cruise altitude (FL350–FL550) would fly through high risk regions; this means that alternative routes should be considered.

The risk-based approach to ash concentrations demonstrates how the four maps of Figure 3 can be condensed into one single figure, which can be used to make fast decisions and overcome the issue of information overload for operators. It can also be used to see why each warning is issued by illustrating which box in the risk matrix a particular location of interest corresponds to. For example, the location annotated with a '+' within the amber region southwest of the British Isles in Figures 7(a) and (b) corresponds to the bottom right box in the ash concentration risk matrix. This means that $\leq$ 10% of the ensemble member simulations resulted in ash concentrations greater than or equal to 4 mg m^{-3} at this location. The risk-based approach allows for multiple layers of information about the ensemble of ash concentration forecasts. This is useful, for example, in an operational environment where a simple colour warning may be required for operators and regulators to take fast or immediate action. Intermediate information is displayed by identifying a location in the risk matrix. This allows decision makers to distinguish between, for example, amber warnings generated from a less likely ($\leq$ 10%), high impact ($\geq$ 4 mg m^{-3}) forecast and a likely (10–90%), medium impact (2–4 mg m^{-3}) forecast.

6.2. Ash dosage risk matrix

The ash concentration risk, however, does not consider the potential risk of flying through low ash concentrations for long durations of exposure or the potential to fly through high ash concentrations for short durations of exposure without experiencing engine damage. To account for these situations a dosage risk matrix was constructed (Figure 5(d)). The ash dosage, D, impact was defined by the following ash dosage boundaries (in g m^{-3} s): $1.44 < D \leq 14.4$, $14.4 < D < 28.8$ and $D \geq 28.8$ and the likelihood ranges were the same as those used for the ash concentration risk matrix.

Figure 7(a) shows the along-route dosage risk corresponding to the dosage risk matrix described above. Visualising the dosage risk along the route shows that an aircraft flying from JFK to LHR return is predicted to encounter a region of high risk towards the end of the eastbound section of the flight. In this case, a flight-planner may decide to 'consider alternative routes' for the aircraft based on the red colour warning (Figure 5(c)).

This method can also be adapted so that both along-route dosage and peak concentration risk are taken into account (Figure 7(b)). In this approach, the risk level corresponding to the higher risk is selected. For example, in the section of the eastbound route between 40 ° W and 30 ° W the peak concentration-based risk is higher than the dosage-based risk and so the route is coloured according to the ash concentration-based risk level. This approach assumes that a high peak concentration should be considered a high risk to the aircraft regardless of the duration of exposure and is therefore more restrictive than using the dosage alone to determine the risk. Current advice from Rolls-Royce is to perform engine checks if an aircraft is suspected to have flown through peak concentrations greater than or equal to 4 mg m^{-3} and that dosages are a more appropriate measure of engine susceptibility to volcanic ash (Clarkson and Simpson, 2017).

Figure 7(c) shows the full range (minimum and maximum) of possible along-route ash concentrations and dosages generated from the ensemble for an aircraft flying through the thick layer level (FL350–FL550) at T+30. The range of dosages produced by the ensemble was from 4.5–2000 g m^{-3} s (median of 160 g m^{-3} s) and the range of peak ash concentrations was from 0–

670 mg m^{-3} (ensemble median maximum of 38 mg m^{-3}). Analysis of the probability density functions (PDFs) of the maxima of the along-route ash concentration and dosage shows that these variables follow lognormal distributions (Figures 8(a), (b)). The along-route ash concentration and dosage ensemble maxima (upper bounds of the shaded regions in Figure 7(c)) are therefore representative of rarely occurring extreme values. The occurrence of extreme values in the ensemble, however, does not preclude the use of a risk matrix. To understand how the risk warning is determined from the distribution of the ensemble, these data can be represented by 'risk PDFs' (Figures 8(c), (d)) using ash concentration and dosage risk matrices. Here the elements of the risk matrix are assigned numerical values (1–9) and the highest risk value intersected by the distribution (re-binned according to the risk matrix impact boundaries) determines the risk level. This approach has recently been suggested for a probabilistic, multi-level wildfire warning system in Chile (Dacre *et al.*, 2018). An alternative, less conservative, approach could be to use the mean or modal risk level. Figures 8(c) and (d) show that while extreme values are present in the ensemble, the majority (> 90%) of the along-route ash concentration and dosage maxima also exceed the maximum impact boundaries of the risk matrices (defined in Sections 6.1 and 6.2). Therefore, one could be confident in a red risk warning issued for the maximum ash concentration and dosage encountered along a return route from JFK-LHR at FL350–FL550 and T+30. The advantage of this third layer of information is that the forecaster can identify when the risk warning is due to outliers (i.e. a small number of ensemble members predicting a high impact) and when the risk warning is confident (i.e. all members predicting the same impact). Thus, even though the LHS dispersion model ensemble members spanned several orders of magnitude in both the along-flight ash concentration and

dosage, the risk-based approach can still be used by flight-planners to make fast and robust decisions.

7. Discussion and conclusions

The methodology described in this paper has been developed to show how a dispersion model ensemble can be used to make fast and robust decisions during a hypothetical Icelandic eruption scenario. The ability to make fast decisions, however, is contingent upon the forecast service organisation having the computer resources necessary to conduct an ensemble forecast in a short period of time. The method was applied to both volcanic ash concentrations and dosages. To permit dosage calculations, aircraft routing software was used to generate time-optimal eastbound and westbound trans-Atlantic flights from New York to London through a simulated ash cloud over the North Atlantic.

To characterise the likelihood of certain ash concentration and dosage thresholds, the concept of model agreement was used. Model agreement values rely on setting ash concentration and dosage thresholds and were shown to be useful in visualising model confidence. Comparison of the control run and the model agreement maps highlighted the importance of quantifying the uncertainty in a deterministic forecast with an ensemble. In an operational context, these maps could be used to plan flight paths closer to the ash cloud boundary in regions where model confidence (agreement) is high than in regions where model confidence is low. This method is an improvement to the subjective approach where the decision-maker infers their own uncertainty by drawing a buffer (typically of uniform distance) around the deterministic ash cloud boundary to indicate their perceived confidence in an ash concentration forecast (e.g. Mulder *et al.*, 2017).

To address the issue of information overload, risk matrices for both ash concentration and dosage were constructed. These were used to demonstrate how fast decisions can be made when taking uncertainty information into consideration. The risk matrix relies upon two key choices: the choice of the likelihood boundaries and the choice of the impact (dosage and/or ash concentration) boundaries. The choice of the likelihood and impact boundaries shown here were based on discussions with aviation stakeholders and illustrate how this method can be implemented. In an operational setting, these boundaries would be set prior to an eruption by the user to reflect their risk appetite. One of the key advantages of this approach is that it allows the user to make decisions even when faced with large sources of uncertainty in the model forecasts. Additionally, visualising the dosage risk along the aircraft's route may be useful on an airline operator fleet-scale where multiple risk routes are viewed on the same map.

The risk-based approach also encompasses varying levels of complexity. As shown with the amber region example, an aircraft pilot may just require a colour warning to respond to the hazard, while a dispersion modelling expert can query further to see what combination of likelihood and impact caused the colour warning. A third step can be taken by looking at risk probability density functions to identify when the risk warning is a result of outliers in the ensemble and when the risk warning is confident. To effectively communicate this approach to aviation stakeholders, the Volcanic Dosage And Risk Tool (VDART) has been developed (accessible at http://www.met.reading.ac.uk/ash-dosage). The VDART interface has been designed as a demonstration tool to illustrate how probabilistic forecasts of ash concentration and dosage risk can be used to make fast and robust decisions. The web-tool was developed in collaboration and consultation with aviation industry regulators, operators, engine manufacturers and the UK Met Office and takes advantage of interactive data visualisation to communicate uncertainty information.

Finally, this approach could potentially be applied to historical eruptions or extended to other aviation hazards such as SO_2 and desert dust dosages or meteorological hazards such as aircraft icing and clear-air turbulence. In cases where the model parameters are well constrained, the ensemble could also be used for post-analysis when an engine manufacturer or airline operator is trying to diagnose the likely range of dosages their engines have been exposed to.

Acknowledgements

This research is funded by Natural Environment Research Council (NERC) under the Environmental Risks to Infrastructure Innovation Programme (NE/P009026/1). Colin Hord, Andy Wells and David Gibbs of the UK Civil Aviation Authority are thanked for explaining the current guidance for flight operations in the vicinity of volcanic ash and for facilitating discussions with the aviation industry. Capt John Monks of British Airways is acknowledged for providing an operators' perspective on flight operations during volcanic ash events. Dr Natalie Harvey (University of Reading) is thanked for providing her expertise on running the NAME model and advice on how to perturb the eruption source and internal model parameters considered in this paper. Dr Helen Thomas (University of Bristol) is thanked for valuable discussions on volcanic ash dosages and comments on the web-tool. The UK Met Office is acknowledged for use of the NAME dispersion model and Drs Matthew Hort, Claire Witham and Frances Beckett (UK Met Office) are thanked for discussions of the results and guidance on the operational LVAAC setup of NAME. Members of the World Meteorological Organization (WMO)/International Union of Geodesy and Geophysics (IUGG) Volcanic Ash Science

Advisory Group (VASAG) are also acknowledged for their constructive comments on the web-tool. Finally, two anonymous reviewers are thanked for their comments which led to significant improvements to the manuscript. NAME simulation output presented in this paper is available on the University of Reading Research Data Archive (accessible at http://dx.doi.org/10.17864/1947.148).

References

Airbus 2017. *Airbus Global Market Forecast 2017–2036 "Growing horizons."* Airbus SAS: Blagnac, France. http://www.airbus.com/content/dam/corporate-topics/publications/backgrounders/Airbus_Global_Market_Forecast_2017-2036_Growing_Horizons_full_book.pdf (accessed 17 November 2017).

Brown A, Milton S, Cullen M, Golding B, Mitchell J, Shelly A 2012. Unified modeling and prediction of weather and climate: A 25-year journey. *B. Am. Meteorol. Soc.* **93**:1865–1877.

Buizza R, Palmer TN 1995. The Singular-Vector Structure of the Atmospheric Global Circulation. *J. Atmos. Sci.* **52**:1434–1456.

Buizza R, Houtekamer PL, Toth Z, Pellerin G, Wei MZ, Zhu YJ 2005. A comparison of the ECMWF, MSC, and NCEP global ensemble prediction systems. *Mon. Weather Rev.* **133**:1076–1097.

Buizza R, Miller M, Palmer TN 1999. Stochastic representation of model uncertainties in the ECMWF Ensemble Prediction System. *Q. J. R. Meteorol. Soc.* **125**:2887–2908.

CAA 2017. *CAP1236: Guidance regarding flight operations in the vicinity of volcanic ash.* Civil Aviation Authority: Aviation House, Gatwick Airport South, UK.

http://publicapps.caa.co.uk/docs/33/CAP%201236%20FEB17.pdf (accessed 17 November 2017).

Casadevall TJ 1994. *Volcanic Ash and Aviation Safety: Proceedings of the First International Symposium on Volcanic Ash and Aviation Safety*. U.S. Geol. Surv. Bull. 2047.

Christmann C, Nunes RR, Schmitt AR, Guffanti M 2017. Flying into Volcanic Ash Clouds: An Evaluation of Hazard Potential. *Science and Technology Organization (STO) - Meeting Proceedings Paper* **MP-AVT-272-KN3**:1–18.

Clarkson RJ, Simpson H 2017. Maximising Airspace Use During Volcanic Eruptions: Matching Engine Durability against Ash Cloud Occurrence. *Science and Technology Organization (STO) - Meeting Proceedings Paper* **MP-AVT-272-17**:1–20.

Clarkson RJ, Majewicz EJE, Mack P 2016. A re-evaluation of the 2010 quantitative understanding of the effects volcanic ash has on gas turbine engines. *Proc. Inst. Mech. Eng. G J. Aerosp. Eng.* **230**:2274–2291.

Cullen MJP 1993. The unified forecast/climate model. *Met. Mag.* **122**:81–94.

Dacre HF, Harvey NJ 2018. Characterising the atmospheric conditions leading to large error growth in volcanic ash cloud forecasts. *Submitted to J. Appl. Meteorol. Climatol.*

Dacre HF, Grant ALM, Hogan RJ, Belcher SE, Thomson DJ, Devenish BJ, Marenco F, Hort MC, Haywood JM, Ansmann A, Mattis I, Clarisse L 2011. Evaluating the structure and magnitude of the ash plume during the initial phase of the 2010 Eyjafjallajökull eruption using lidar observations and NAME simulations. *J. Geophys. Res.* **116**:D00U03.

Dacre HF, Grant ALM, Johnson BT 2013. Aircraft observations and model simulations of concentration and particle size distribution in the Eyjafjallajökull volcanic ash cloud. *Atmos. Chem. Phys.* **13**:1277–1291.

Dacre HF, Grant ALM, Harvey NJ, Thomson DJ, Webster HN, Marenco F 2015. Volcanic ash layer depth: Processes and mechanisms. *Geophys. Res. Lett.* **42**:637–645.

Dacre HF, Crawford BR, Charlton-Perez AJ, Lopez-Saldana G, Griffiths GH, Vicencio Veloso J 2018. Chilean wildfires: Probabilistic prediction, emergency response and public communication. *B. Am. Meteorol. Soc.* BAMS–D–17–0111.1.

Devenish BJ, Francis PN, Johnson BT, Sparks RSJ, Thomson DJ 2012. Sensitivity analysis of dispersion modeling of volcanic ash from Eyjafjallajökull in May 2010. *J. Geophys. Res. Atmos.* **117**:D00U21.

Folch A 2012. A review of tephra transport and dispersal models: Evolution, current status, and future perspectives. *J. Volcanol. Geoth. Res.* **235-236**:96–115.

Gneiting T, Raftery AE 2005. Weather forecasting with ensemble methods. *Science* **310**:248–249.

Guffanti M, Tupper A 2015. Volcanic Ash Hazards and Aviation Risk. In: *Volcanic Hazards, Risks and Disasters*. Elsevier, 87–108.

Guffanti M, Casadevall TJ, Budding K 2010. Encounters of aircraft with volcanic ash clouds; a compilation of known incidents, 1953-2009. *U.S. Geol. Surv. Data Ser.* **545**:1–16.

Harvey NJ, Huntley N, Dacre HF, Goldstein M, Thomson D, Webster H 2018. Multi-level emulation of a volcanic ash transport and dispersion model to quantify sensitivity to uncertain parameters. *Nat. Hazards Earth Syst. Sci.* **18**:41–63.

ICAO 2007. *Doc 9691 AN/954: Manual on Volcanic Ash, Radioactive Material and Toxic Chemical Clouds, Second Edition – 2007.* International Civil Aviation Organization: Montréal, Quebec, Canada. https://skybrary.aero/bookshelf/books/2997.pdf (accessed 5 February 2018).

ICAO 2016. *Volcanic Ash Contingency Plan, European and North Atlantic Regions. EUR Doc. 019, NAT Doc. 006, Part II. Edition 2.0.0 – July 2016.* International Civil Aviation Organization: Neuilly-sur-Seine, France. https://www.icao.int/EURNAT/EUR%20and%20NAT%20Documents/EUR+NAT%20VACP.pdf (accessed 26 February 2018).

Iman RL, Conover WJ 1980. Small sample sensitivity analysis techniques for computer models, with an application to risk assessment. *Commun. Stat. Part A* **9**:1749–1842.

Irvine EA, Hoskins BJ, Shine KP, Lunnon RW, Froemming C 2013. Characterizing North Atlantic weather patterns for climate-optimal aircraft routing. *Meteorol. Appl.* **20**:80–93.

Irvine EA, Shine KP, Stringer MA 2016. What are the implications of climate change for trans-Atlantic aircraft routing and flight time? *Transp. Res. D: Transp. and Environ.* **47**:44–53.

Jones A, Thomson D, Hort M, Devenish B 2007. The U.K. Met Office's Next-Generation Atmospheric Dispersion Model, NAME III. In: *Air Pollution Modeling and Its Application XVII*. Boston, MA: Springer US, 580–589.

Kristiansen NI, Prata AJ, Stohl A 2015. Stratospheric volcanic ash emissions from the 13 February 2014 Kelut eruption. *Geophys. Res. Lett.* **42**:588–596.

Lawrence BN, Bennett VL, Churchill J, Juckes M, Kershaw P, Oliver P, Pritchard M, Stephens A 2012. The JASMIN super-data-cluster. *arXiv:1204.3553 [cs.DC]*.

Lunnon RW, Marklow AD 1992. Optimization of Time Saving in Navigation Through an Area of Variable Flow. *J. Navig.* **45**:384–399.

Mastin LG, Guffanti M, Servranckx R, Webley P, Barsotti S, Dean K, Durant A, Ewert JW, Neri A, Rose WI, Schneider D, Siebert L, Stunder B, Swanson G, Tupper A, Volentik A, Waythomas CF 2009. A multidisciplinary effort to assign realistic source parameters to models of volcanic ash-cloud transport and dispersion during eruptions. *J. Volcanol. Geoth. Res.* **186**:10–21.

Millington SC, Saunders RW, Francis PN, Webster HN 2012. Simulated volcanic ash imagery: A method to compare NAME ash concentration forecasts with SEVIRI imagery for the Eyjafjallajkull eruption in 2010. *J. Geophys. Res. Atmos.* **117**:D00U17.

Mulder KJ, Lickiss M, Harvey N, Black A, Charlton-Perez A, Dacre H, McCloy R 2017. Visualizing Volcanic Ash Forecasts: Scientist and Stakeholder Decisions Using Different Graphical Representations and Conflicting Forecasts. *Wea. Climate Soc.* **9**:333–348.

Neal RA, Boyle P, Grahame N, Mylne K, Sharpe M 2014. Ensemble based first guess support towards a risk-based severe weather warning service. *Meteorol. Appl.* **21**:563–577.

Palmer TN 2002. The economic value of ensemble forecasts as a tool for risk assessment: From days to decades. *Q. J. R. Meteorol. Soc.* **128**:747–774.

Peterson RA, Dean KG 2007. Forecasting exposure to volcanic ash based on ash dispersion modeling. *J. Volcanol. Geoth. Res.* **170**:230–246.

Prata AJ, Prata AT 2012. Eyjafjallajökull volcanic ash concentrations determined using Spin Enhanced Visible and Infrared Imager measurements. *J. Geophys. Res. Atmos.* **117**:D00U23.

Prata AJ, Tupper A 2009. Aviation hazards from volcanoes: The state of the science. *Nat. Hazards* **51**:239–244.

Prata AJ, Kristiansen N, Thomas HE, Stohl A 2018. Ash metrics for European and trans-Atlantic air routes during the Eyjafjallajökull eruption 14 April-23 May, 2010. *J. Geophys. Res. Atmos.*

Rolls-Royce 2017. *All RB211 and Trent Engines - Volcanic Ash Limits Guidance.* Rolls-Royce plc: Derby, UK. https://www.wmo.int/aemp/sites/default/files/VA_Limits_Guidance_Rolls-Royce.pdf (accessed 17 November 2017).

Stohl A, Prata AJ, Eckhardt S, Clarisse L, Durant A, Henne S, Kristiansen NI, Minikin A, Schumann U, Seibert P, Stebel K, Thomas HE, Thorsteinsson T, Tørseth K, Weinzierl B 2011. Determination of time- and height-resolved volcanic ash emissions and their use for quantitative ash dispersion modeling: the 2010 Eyjafjallajökull eruption. *Atmos. Chem. Phys.* **11**:4333–4351.

Webster HN, Thomson DJ, Johnson BT, Heard IPC, Turnbull K, Marenco F, Kristiansen NI, Dorsey J, Minikin A, Weinzierl B, Schumann U, Sparks RSJ, Loughlin SC, Hort MC, Leadbetter SJ, Devenish BJ, Manning AJ, Witham CS, Haywood JM, Golding BW 2012. Operational prediction of ash concentrations in the distal volcanic cloud from the 2010 Eyjafjallajökull eruption. *J. Geophys. Res. Atmos.* **117**:D00U08.

Witham CS, Webster HN, Hort MC, Jones A, Thomson D 2012. Modelling concentrations of volcanic ash encountered by aircraft in past eruptions. *Atmos. Environ.* **48**:219–229.

Witham CS, Hort MC, Thomson D, Leadbetter SJ, Devenish BJ, Webster HN, Beckett FM 2016. The current volcanic ash modelling set-up at the London VAAC. *Met Office Technical Summary (v1.3)*:1–9.

Wylie S, Bucknell A, Forsyth P, McGilvray M, Gillespie DRH 2017. Reduction in Flow Parameter Resulting From Volcanic Ash Deposition in Engine Representative Cooling Passages. *J. Turbomach.* **139**:031008.

Tables

Parameter	Control value	Sampling range
Plume height (km)	15	13 to 17
Mass eruption rate factor	1	1/3 to 3
Source duration (h)	16	6 to 26
Source timing (UTC)	0300 1 Jan 2017	0300 to 1300 1 Jan 2017
Distal fine ash fraction (%)	5	1 to 10
Horizontal (vertical) Lagrangian timescale (τ) for free tropospheric turbulence (s)	300 (100)	100 to 900 (33.33 to 300)
Standard deviation (σ) of horizontal (vertical) velocity for free tropospheric turbulence (m s^{-1})	0.25 (0.10)	0.0025 to 2.5 (0.001 to 1)
Standard deviation (σ) of horizontal velocity for unresolved mesoscale motions (m s^{-1})	0.8	0.27 to 1.74
Meteorological fields	MetUM analysis	ECMWF members 0 to 19

Table 1. Control run parameters selected for Latin Hypercube Sampling.

Figures

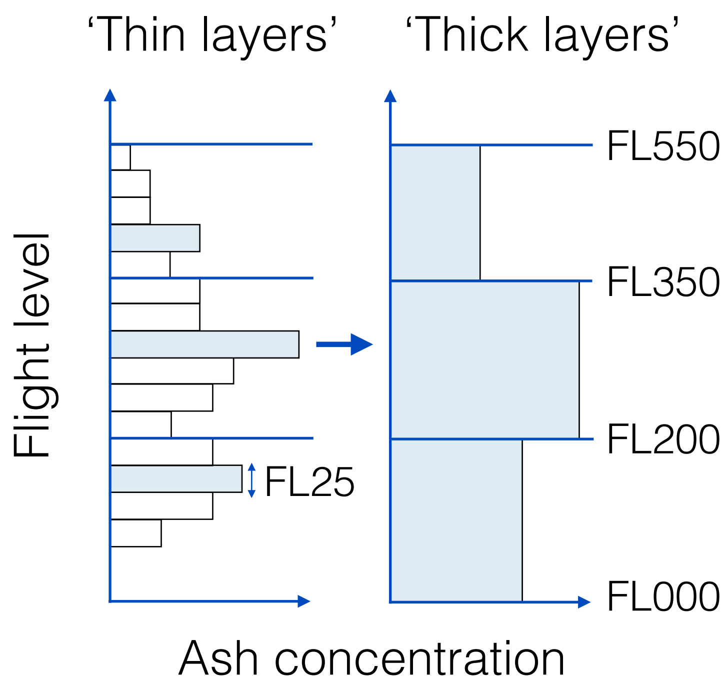

Figure 1. Schematic showing the difference between the thin layer and thick layer LVAAC setup of NAME.

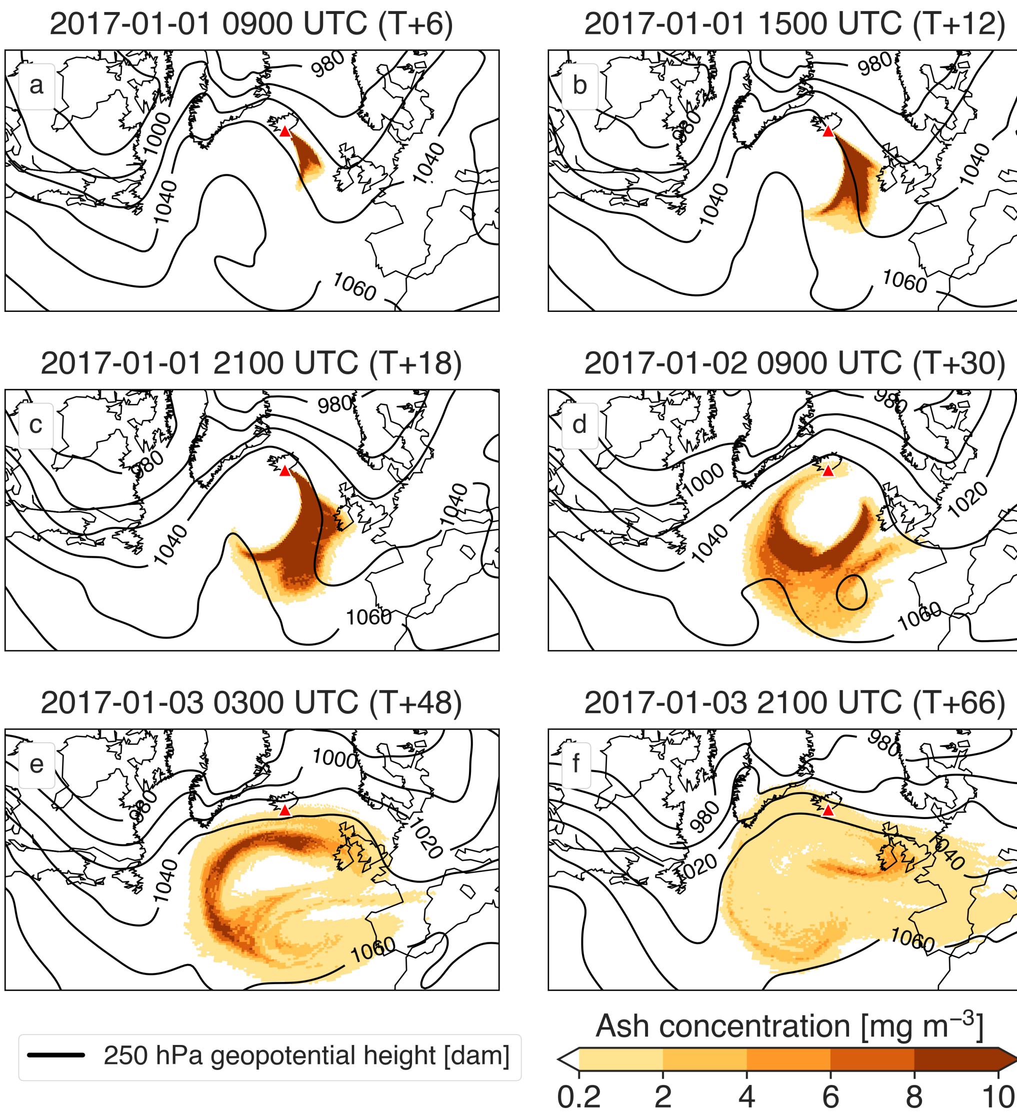

Figure 2. Ash concentrations for the control run simulation for the Katla (indicated by the red triangle) eruption scenario with 250 hPa geopotential height contours overlaid. The control run start time is 0300 UTC on 1 January 2017. Concentrations have been post-processed to produce the LVAAC's thick layer product from FL350–FL550. (a) 6, (b) 12, (c) 18, (d) 30, (e) 48, (f) 66 hours after eruption.

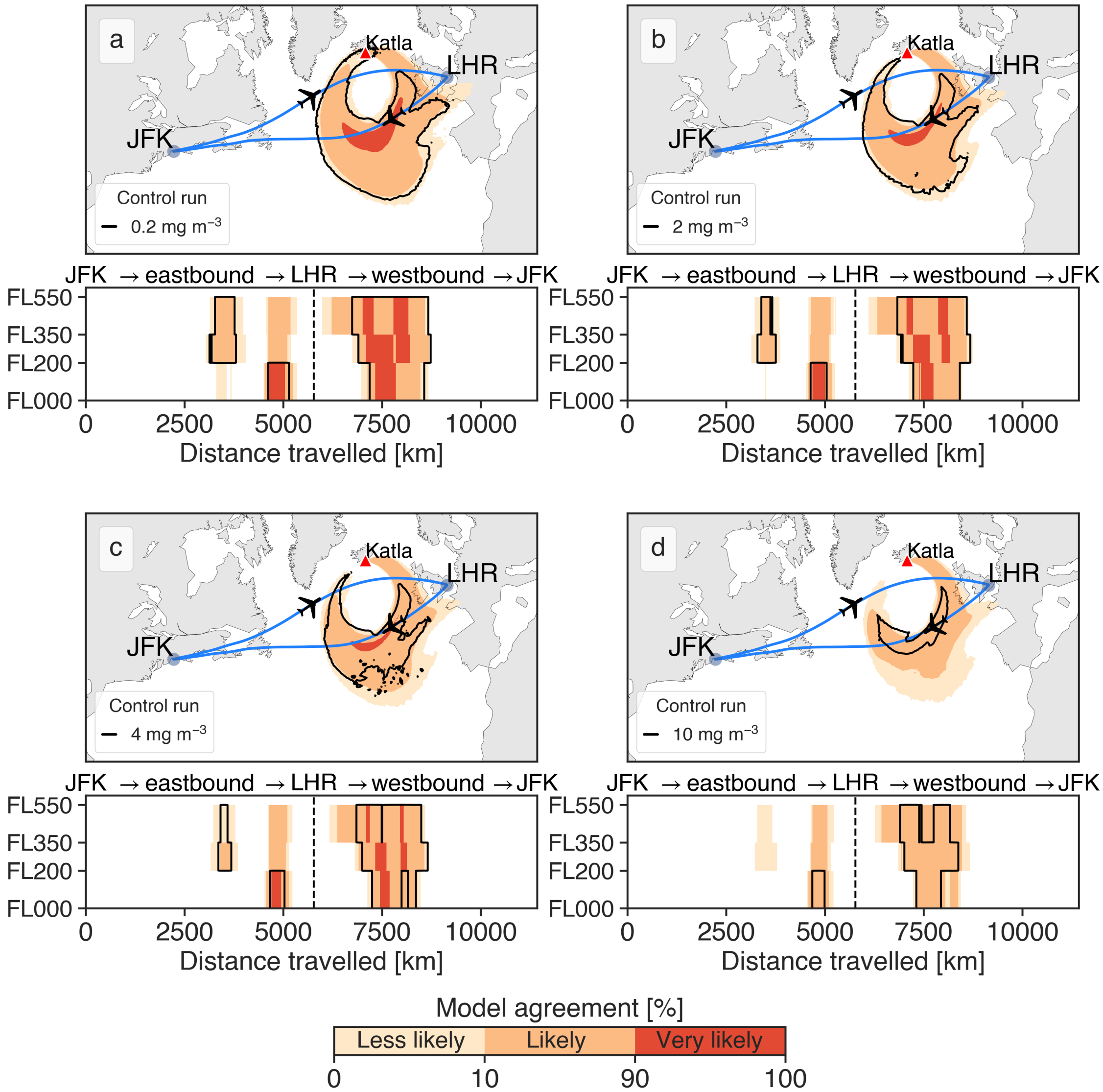

692

693 Figure 3. Percentage of ensemble members at T+30 that resulted in ash concentrations above (a) 0.2 mg m^{-3}, (b) 2
694 mg m^{-3}, (c) 4 mg m^{-3} and (d) 10 mg m^{-3}. Each panel shows the geographic model agreement and the relevant ash
695 concentration contour for the control run (black line) at the FL350–FL550 thick layer level (top) and the vertical
696 cross-section of model agreement and the relevant ash concentration contour along the JFK–LHR and LHR–JFK
697 time-optimal routes (bottom).

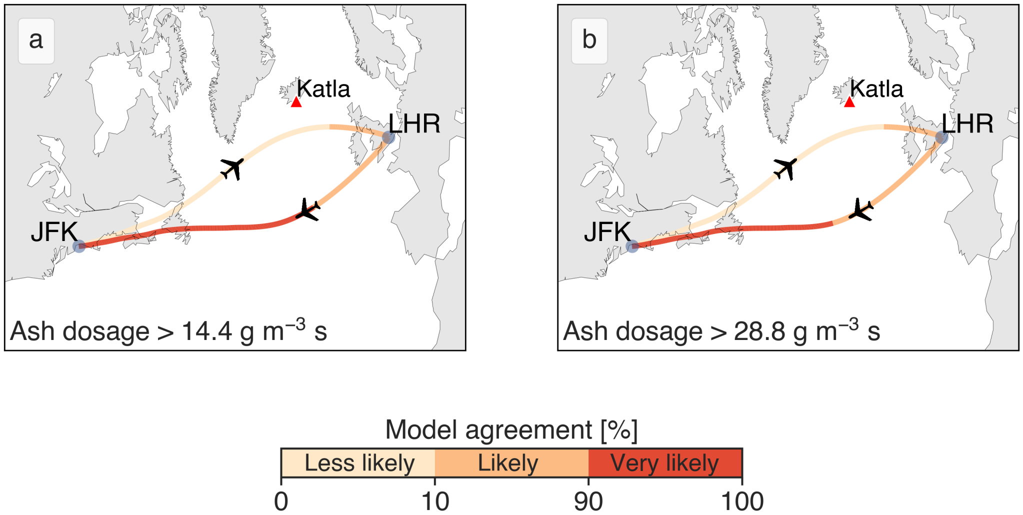

Figure 4. Percentage of ensemble members that resulted in ash dosages above (a) 14.4 g m^{-3} s and (b) 28.8 g m^{-3} s. Percentages have been calculated along the time-optimal eastbound and westbound flight routes between JFK and LHR at T+30 for the FL350–FL550 thick layer level.

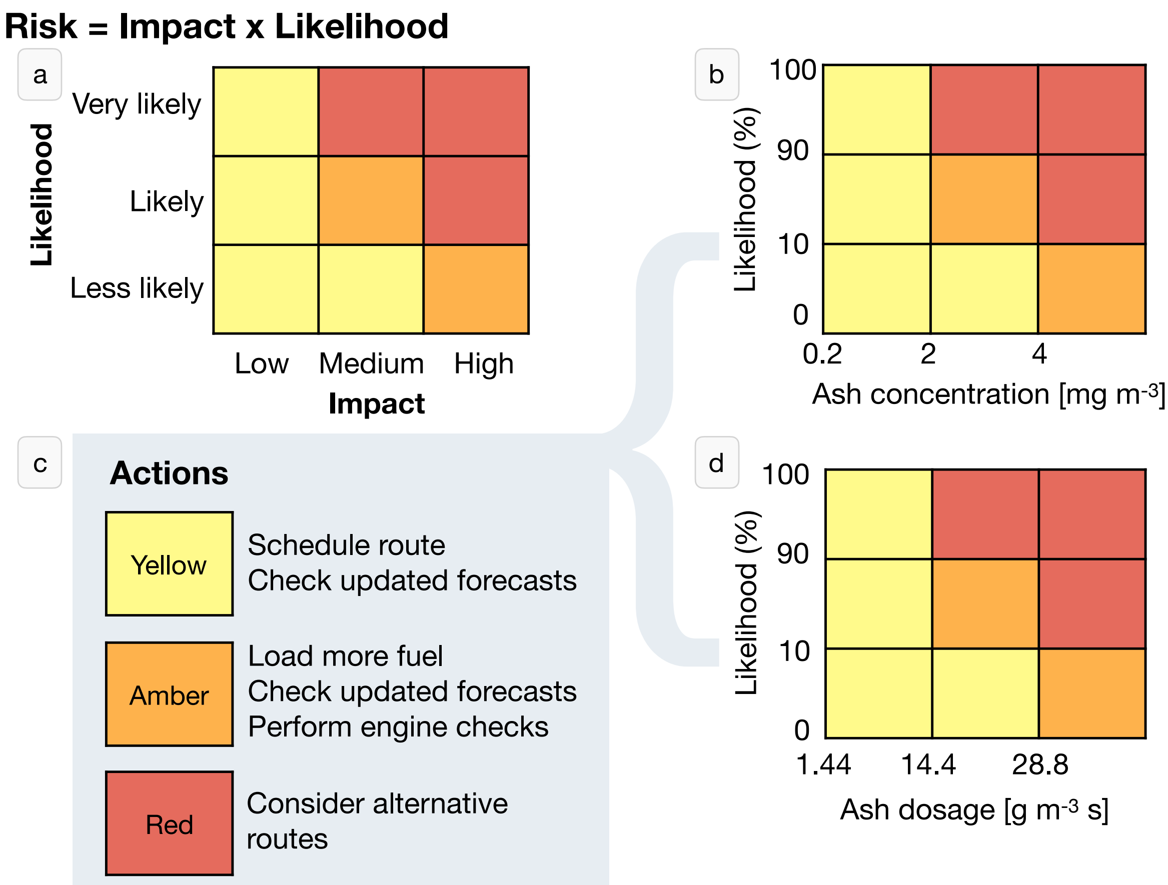

703

704 Figure 5. Schematic showing (a) a generic risk matrix, (b) how the ash concentration risk matrix was constructed, (c)
705 example actions that could be taken by a decision-maker in response to a yellow, amber or red warning and (d) how
706 the ash dosage risk matrix was constructed.

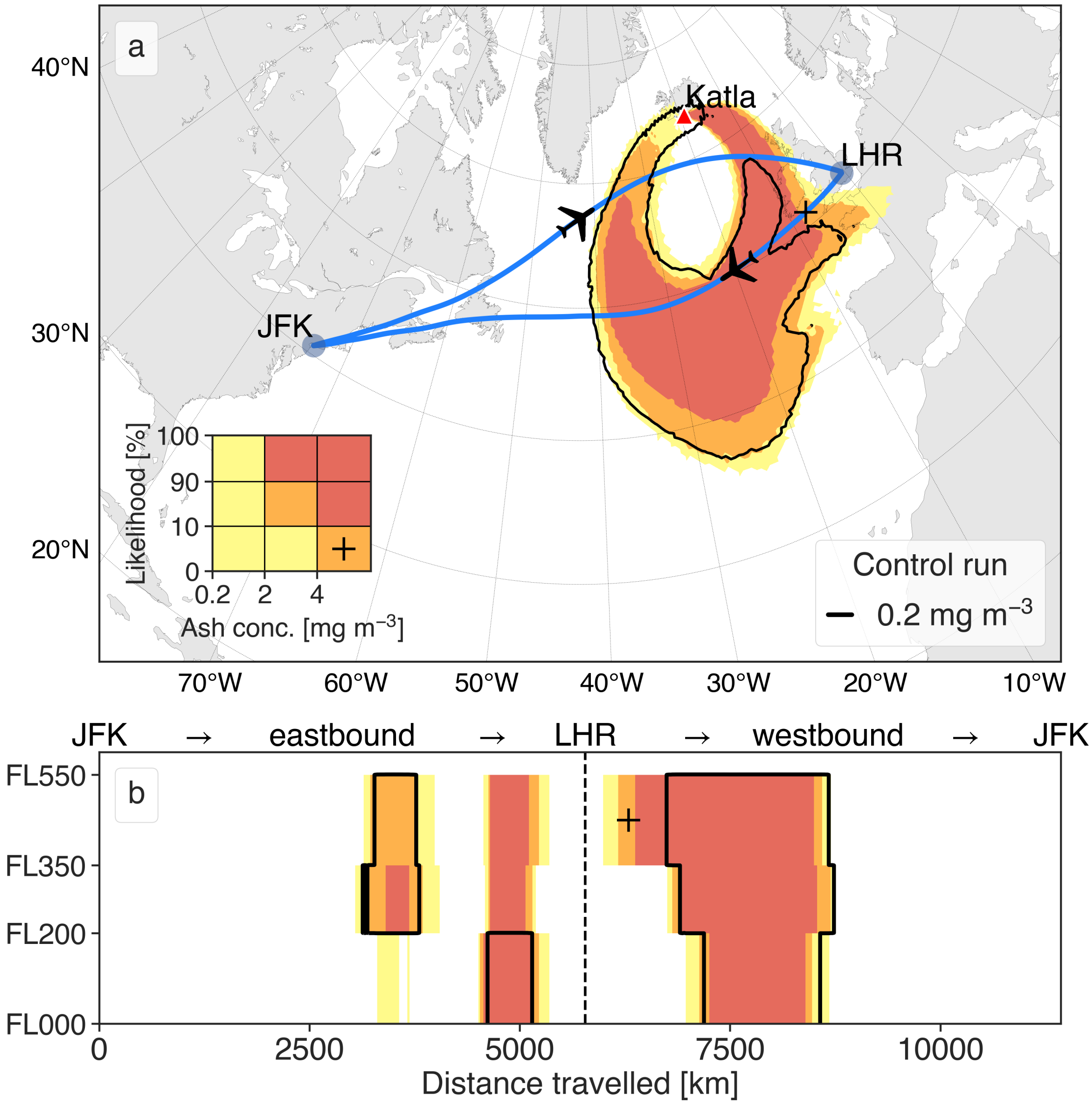

Figure 6. (a) Horizontal ash concentration risk map for the thick layer level (FL350–FL550) at T+30. (b) Vertical risk maps for each thick layer corresponding to the return JFK–LHR route (plotted on (a)) at T+30. The '+' annotated on the risk matrix (inset of (a)) corresponds to the risk level at the location of the '+' on (a) and (b).

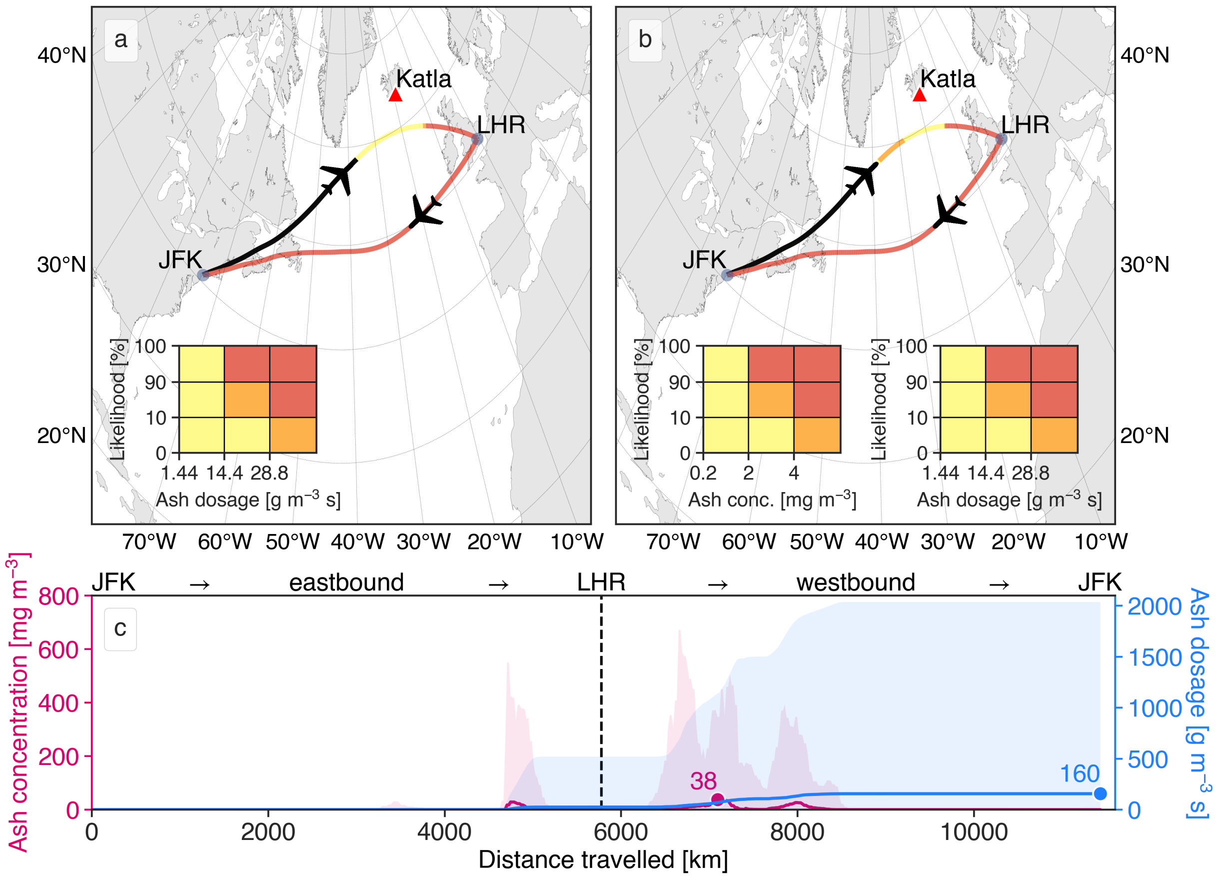

711

712 Figure 7. (a) Dosage risk for the New York (JFK) to London (LHR) trans-Atlantic air-route at T+30 and thick layer level FL350–FL550. (b) Dosage and ash concentration risk for the same route in (a). (c) Along-route ash concentration and dosage. Values annotated are the ensemble median maximum values correct to two significant figures; shaded regions correspond to minimum and maximum of the ash concentration and dosage.

716

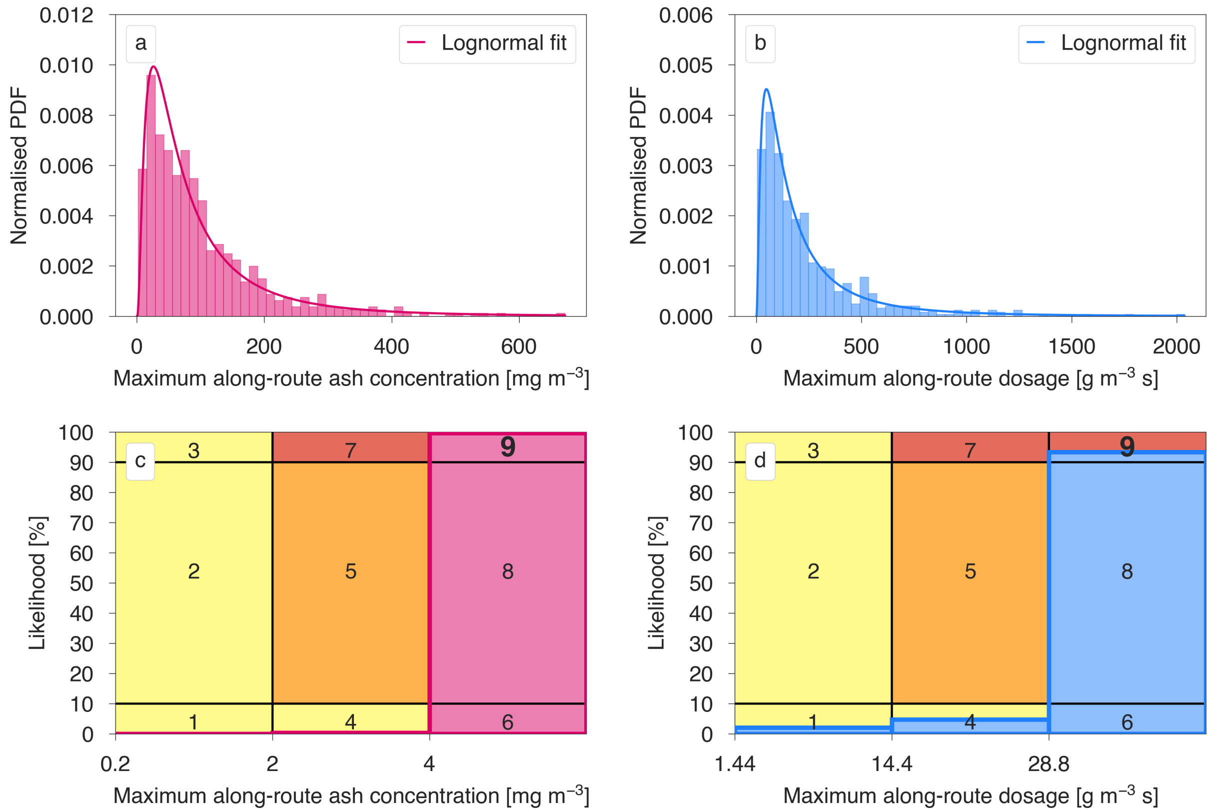

Figure 8. Normalised probability density functions (PDFs) of the maxima of the (a) along-route ash concentration and (b) along-route dosage for the return air-route from New York (JFK) to London (LHR) at T+30 and thick layer level FL350–FL550 (lines plotted over each histogram indicate a Lognormal distribution fit). The 'risk PDFs' corresponding to the distributions shown in (a) and (b) are illustrated in (c) and (d), respectively. Note that the numerical values annotated on (c) and (d) indicate the risk level, with the risk issued shown in bold). The pink and blue histograms plotted over the risk matrix have been re-binned according to the impact boundaries shown in Figure 5.